

Polarization transfer in the inner-shell photoionization of sodiumlike ions

L. Sharma,^{1,2} A. Surzhykov,^{1,2} M. K. Inal,³ and S. Fritzsche^{2,4}

¹*Physikalisches Institut, Universität Heidelberg, Philosophenweg 12, DE-69120 Heidelberg, Germany*

²*GSI Helmholtzzentrum für Schwerionenforschung GmbH, Planckstrasse 1, DE-64291 Darmstadt, Germany*

³*Département de Physique, Université A. Belkaid, Boîte Postale 119, 13000 Tlemcen, Algeria*

⁴*Department of Physics, Post Office Box 3000, FI-90014 University of Oulu, Finland*

(Received 11 December 2009; published 23 February 2010)

The inner-shell photoionization of highly charged ions is studied, together with their subsequent radiative decay, within the framework of the density matrix theory and the multiconfiguration Dirac-Fock (MCDF) approach. For the subsequent radiative decay of the ions, we investigate in particular how the linear polarization of characteristic radiation is affected if the incident light is itself polarized. Detailed calculations are performed for the $2p^5 3s \rightarrow 2p^6$ radiative transitions following the production of a $2p$ vacancy in the sodiumlike Fe^{15+} , W^{63+} , and U^{81+} ions. From these calculations, it is shown that the (degree of) linear polarization of the characteristic radiation may be enhanced by a factor of 2 due to the polarization transfer from the incident light.

DOI: 10.1103/PhysRevA.81.023419

PACS number(s): 32.80.Fb, 32.50.+d, 32.30.Rj

I. INTRODUCTION

The ionization of inner-shell electrons in atoms and ions results in the formation of excited ionic states that may stabilize subsequently by the emission of one (or several) characteristic photons. In this deexcitation, angular and polarization properties of this decay radiation are directly related to the magnetic sublevel population of the excited ion and, hence, to the dynamics of a particular ionization process [1–3]. A number of studies, both in experiment and theory, have therefore been performed during the last decades in order to analyze the characteristic emission and to improve our understanding of collisional behavior of ions and atoms. Following an electron-impact excitation, for example, recent investigations of the angular distribution and linear polarization of fluorescent photons revealed important information on the properties of high-temperature laboratory and astrophysical plasmas [4–9]. In high- Z domain, moreover, a polarization analysis of characteristic x-ray lines provided detailed insight into the relativistic and many-body phenomena in energetic atomic collisions [6–8, 10, 11].

Besides the vacancy production caused by the electron impact, the inner-shell *photoionization* of ions (and atoms) has attracted particular attention during the recent years. This process plays an important role for astrophysical plasmas located in the vicinity of strong radiation sources such as accretion disks and binary stars [12–14]. Moreover, owing to the recent advances in developing heavy-ion traps and intensive light sources in the extreme ultraviolet (EUV) and x-ray domain, inner-shell ionization processes of high- Z ions will be observed soon experimentally and will provide a new route for studying relativistic and nondipole effects in heavy atomic systems.

A theoretical analysis of the “photoionization plus decay” process has been performed recently by Inal and co-workers [15], who placed special emphasis on the linear polarization of the $2p^5 3s$ - $2p^6$ characteristic emission from neonlike Fe^{16+} and U^{82+} ions following $2p$ vacancy production. In that work, detailed calculations were carried out to explore both the energy dependence of the (degree of) polarization and the effects which arise from the higher nondipole terms in

the expansion of the electron-photon interaction. In contrast, the (expected) dependence on the polarization of incoming radiation was not discussed in Ref. [15], in which analysis was restricted to the vacancy production by unpolarized light only. The information about the “polarization transfer” in the inner-shell photoionization, however, is of great importance to the diagnostics of many laboratory and astrophysical plasmas. They are required to understand the ongoing measurements on laboratory plasmas exposed to polarized x-ray emission from Z pinches [16–21]. Moreover, many astrophysical x-ray sources such as magnetized neutron stars [22] or black-hole accretion disks [23] are expected to emit strongly polarized light. Detailed information about polarization properties of this light (and, hence, about its sources) may be obtained by studying the linear polarization of characteristic lines as emitted from ionized plasma clouds [24].

In this contribution, we apply the density matrix formalism to analyze the linear polarization of characteristic photons following the inner-shell ionization of ions by polarized incident radiation. Before presenting details of the theory, we first summarize in Sec. II the geometry under which the two-step “ionization plus decay” process is to be considered. Attention is paid especially to the choice of the quantization axis with respect to which one explores magnetic sublevel population of the excited ion. As discussed in Sec. III A, such a population is described most naturally in terms of statistical tensors. The general expression for these tensors is derived by taking into account the full multipole decomposition for the electron-photon interaction operator. While this expression can be employed to analyze photoproduction of excited ionic states for an arbitrary polarization state of the incident light, in Sec. III B we restrict our analysis to the case of linearly polarized radiation. By utilizing the statistical tensors obtained for this particular experimental “setup,” we will derive in Sec. III C the polarization Stokes parameters for the x-ray photons as emitted in the radiative decay of the excited ion states. In Sec. IV, these Stokes parameters are then calculated in the framework of the multiconfiguration Dirac-Fock (MCDF) method. In particular, detailed computations have been carried out for the two electric-dipole transitions $2p^5 3s \ ^1P_1 \rightarrow 2p^6 \ ^1S_0$ and $2p^5 3s \ ^3P_1 \rightarrow 2p^6 \ ^1S_0$ as well as

the magnetic quadrupole transition $2p^5 3s \ ^3P_2 \rightarrow 2p^6 \ ^1S_0$ following the photoionization of the $2p$ electron of the sodiumlike Fe^{15+} , W^{63+} , and U^{81+} ions. As seen from these computations, polarization of the incident light generally leads to an enhancement by about a factor of 2 for all three characteristic lines. For high photon energies, however, such a ‘‘polarization transfer’’ phenomenon is almost reversed by the cascade feeding of the excited $2p^5 3s$ ionic states from the higher-lying levels. Even though the theoretical analysis of the photoionization of sodiumlike species is the major topic of this paper, we have also briefly discussed the $2p$ vacancy production and decay of (initially) magnesiumlike uranium ions. Relativistic calculations performed for these ions have again indicated a significant ‘‘polarization transfer’’ effect which becomes most pronounced for the near-threshold energies. A brief summary of these results is given finally in Sec. VI.

II. GEOMETRY

To explore polarization transfer in the two-step ‘‘photoionization plus subsequent decay’’ process, we shall first agree on the geometry under which the emission of the characteristic photons is observed. For vacancy production by linearly polarized incident light, the photon wave vector \mathbf{k} and polarization vector $\boldsymbol{\epsilon}$ determine two preferred directions of the overall system. The choice of the quantization (z) axis along either of these two directions allows us to define two (slightly different) geometric setups displayed in Fig. 1.

In the first geometry (see left panel of the figure), we adopt the quantization (z) axis along the direction \mathbf{k} of the incident light, while the x axis is taken along the polarization vector $\boldsymbol{\epsilon}$. As we will see later in Sec. III A, such a choice simplifies the multipole expansion of the electron-photon interaction operator and, hence, results in much faster evaluation of the statistical tensors of the excited ionic states. In atomic photoionization calculations, however, another coordinate system is usually employed with the z axis directed along the polarization vector $\boldsymbol{\epsilon}$ and the x axis directed along the propagation direction \mathbf{k} [25] (see right panel of Fig. 1).

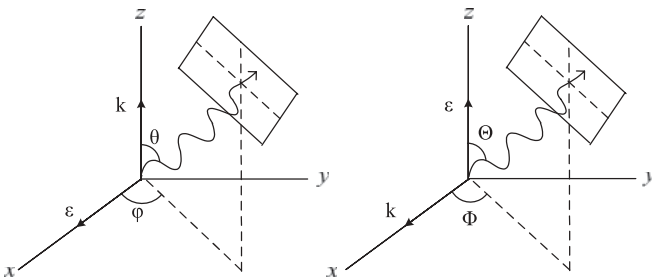


FIG. 1. Two geometries for the inner-shell ionization of an ion by linearly polarized incoming light, and for their subsequent radiative decay. Left: the ionizing radiation comes along the z axis with the polarization vector aligned in the x direction, and the emission direction of the characteristic photons is described by two angles (θ, ϕ) . Right: the ionizing radiation comes along the x axis with the polarization vector aligned in the z direction, while the emission direction of the characteristic photons is described by two angles (Θ, Φ) .

The quantization of the system along the vector $\boldsymbol{\epsilon}$ requires longer computation time but makes an easier analysis of the polarization properties of the subsequent decay photons [26].

III. THEORY

A. Density matrix formalism

Having defined the geometry of the two-step ‘‘ionization plus decay’’ process, we recall next the basic formulas which one needs to characterize the population of the excited (intermediate) states of the ion. Most naturally, this population can be described within the framework of the density matrix theory. In this theory, one adopts the language of the so-called statistical operators to represent the various quantum states of the overall system and to accompany such a system through the collision process. For the inner-shell photoionization, the statistical operator $\hat{\rho}_i$ of the initial state is just given by the direct product of the operators of the atom (ion) and the incident photon:

$$\hat{\rho}_i = \hat{\rho}_{\text{ion}} \otimes \hat{\rho}_\gamma. \quad (1)$$

The explicit form of this operator depends, of course, on the particular representation that is chosen to specify states of the two subsystems. In particular, we will employ here the *helicity* representation of the photon statistical operator:

$$\hat{\rho}_\gamma = \sum_{\lambda\lambda'} c_{\lambda\lambda'} |\mathbf{k}\lambda\rangle \langle \mathbf{k}\lambda'|, \quad (2)$$

where \mathbf{k} is the wave vector and $\lambda = \pm 1$ is the spin projection of the photon onto the direction of its propagation. In Eq. (2), moreover, a set of parameters $c_{\lambda\lambda'}$ uniquely defines the (degree and direction of) polarization of the incoming radiation. For further theoretical analysis, it is convenient to express $c_{\lambda\lambda'}$ in terms of the so-called Stokes parameters [1,2]:

$$c_{\lambda\lambda'} = \langle \mathbf{k}\lambda | \hat{\rho}_\gamma | \mathbf{k}\lambda' \rangle = \frac{1}{2} \begin{pmatrix} 1 + P_3 & P_1 - iP_2 \\ P_1 + iP_2 & 1 - P_3 \end{pmatrix}, \quad (3)$$

which are often utilized in experiments in order to characterize both the linear (P_1 and P_2) and circular (P_3) polarization of the light.

Apart from $\hat{\rho}_\gamma$, the statistical operator $\hat{\rho}_{\text{ion}}$ of the ion *prior* to the ionization still has to be specified in order to define completely the initial state (1) of the combined system ‘‘atom plus photon.’’ If we assume the ion to be initially in an unpolarized state $|\alpha_i J_i\rangle$ with well-defined total angular momentum J_i and with α_i standing for all additional quantum numbers, its statistical operator can be written as

$$\hat{\rho}_{\text{ion}} = \frac{1}{2J_i + 1} \sum_{M_i} |\alpha_i J_i M_i\rangle \langle \alpha_i J_i M_i|, \quad (4)$$

where summation runs over all magnetic quantum numbers M_i .

In the ‘‘intermediate’’ state of the system, after absorption of the photon, we have a continuum electron with asymptotic momentum \mathbf{p} and spin projection m_s , as well as an ion in the excited state $|\alpha_f J_f\rangle$. Statistical operator $\hat{\rho}_f$ of such a state can be obtained from the initial-state operator (1) owing to the relation

$$\hat{\rho}_f = \hat{R} \hat{\rho}_i \hat{R}^\dagger, \quad (5)$$

where \hat{R} is the transition operator that describes the interaction of the electrons with the radiation field. It can be written as a sum of one-particle operators:

$$\hat{R}(\mathbf{k}) = \sum_n \hat{R}_n(\mathbf{k}) = \sum_n \boldsymbol{\alpha}_n \cdot \mathbf{u}_\lambda e^{i\mathbf{k}\cdot\mathbf{r}_n}, \quad (6)$$

where $\boldsymbol{\alpha}_n = (\alpha_{x,n}, \alpha_{y,n}, \alpha_{z,n})$ denotes the vector of the Dirac matrices for the n th particle and \mathbf{u}_λ is the polarization vector of the photon.

Equation (5) describes the ‘‘intermediate’’ density operator and, thus, contains all the information about the system following the inner-shell photoionization of the ion (atom). Instead of using the density operator $\hat{\rho}_f$, however, it is often more convenient to work with its matrix representation, briefly referred to as the intermediate-state density matrix. In a basis with well-defined angular momenta, this density matrix is given by

$$\begin{aligned} & \langle \alpha_f J_f M_f, \mathbf{p}m_s | \hat{\rho}_f | \alpha_f J_f M'_f, \mathbf{p}m'_s \rangle \\ &= \sum_{M_i M'_i \lambda \lambda'} \langle \alpha_f J_f M_f, \mathbf{p}m_s | \hat{R} | \alpha_i J_i M_i, \mathbf{k}\lambda \rangle \langle \alpha_i J_i M_i, \mathbf{k}\lambda | \hat{\rho}_i \\ & \quad \times | \alpha_i J_i M'_i, \mathbf{k}\lambda' \rangle \langle \alpha_i J_i M_i, \mathbf{k}\lambda' | \hat{R}^\dagger | \alpha_f J_f M'_f, \mathbf{p}m'_s \rangle \\ &= \frac{1}{2J_i + 1} \sum_{M_i \lambda \lambda'} c_{\lambda \lambda'} \langle \alpha_f J_f M_f, \mathbf{p}m_s | \\ & \quad \times \sum_n \boldsymbol{\alpha}_n \cdot \mathbf{u}_{\lambda,n} e^{i\mathbf{k}\cdot\mathbf{r}_n} | \alpha_i J_i M_i \rangle \langle \alpha_f J_f M'_f, \mathbf{p}m'_s | \\ & \quad \times \sum_n \boldsymbol{\alpha}_n \cdot \mathbf{u}_{\lambda',n} e^{i\mathbf{k}\cdot\mathbf{r}_n} | \alpha_i J_i M_i \rangle, \end{aligned} \quad (7)$$

where we made use of the statistical operators of the incident photon beam (2) and the initial ion (4).

As seen from Eq. (7), any further analysis of the intermediate-state density matrix requires the simplification of the transition amplitude $\langle \alpha_f J_f M_f, \mathbf{p}m_s | \hat{R} | \alpha_i J_i M_i \rangle$. This can be achieved by performing a decomposition of both the photon and the continuum wave functions into partial waves. As discussed previously [27], the particular form of such a decomposition depends on the choice of the quantization (z) axis. By adopting, for instance, the quantization axis along the incoming photon momentum, we can express free-electron wave in terms of its partial waves as

$$| \mathbf{p}m_s \rangle = \sum_{\kappa m_j} i^l e^{-i\Delta_\kappa} \langle lm_l 1/2m_s | jm_j \rangle Y_{lm_l}^*(\hat{\mathbf{p}}) | \epsilon l j m_j \rangle, \quad (8)$$

where we need to perform a rotation of the spatial part of the electron wave function from the z axis to the $\hat{\mathbf{p}}$ direction. Moreover, the summation in Eq. (8) runs over all partial waves $\kappa = \pm 1, \pm 2, \dots$, i.e., along all values of the Dirac angular momentum quantum number $\kappa = \pm(j + 1/2)$ for $l = j \pm 1/2$. In this notation, the (nonrelativistic orbital) momentum l now represents the parity of the partial waves $| \epsilon l j m_j \rangle$, and Δ_κ is the Coulomb phase shift.

To obtain next the partial-wave expansion of the *many-electron* scattering states in the intermediate density matrix (7), we combine Eq. (8) with the standard procedure for the

coupling of two angular momenta [28]:

$$\begin{aligned} | \alpha_f J_f M_f, \mathbf{p}m_s \rangle &= \mathcal{A} \sum_{\kappa m_j} i^l e^{-i\Delta_\kappa} \langle lm_l 1/2m_s | jm_j \rangle \\ & \quad \times Y_{lm_l}^*(\hat{\mathbf{p}}) \sum_{JM} \langle J_f M_f jm_j | JM \rangle \\ & \quad \times | (\alpha_f J_f, \epsilon l j) JM \rangle, \end{aligned} \quad (9)$$

where the operator \mathcal{A} is used to ensure the proper antisymmetrization of the emitted photoelectron wave with respect to the bound-state orbitals.

Apart from the continuum electron wave function (8), we shall also expand the one-particle interaction operators $\hat{R}_n(\mathbf{k})$ in terms of spherical tensors, i.e., in terms of electric and magnetic multipole fields. By using a quantization axis along the photon momentum, this decomposition reads as [28]

$$\mathbf{u}_\lambda e^{i\mathbf{k}\cdot\mathbf{r}} = \sqrt{2\pi} \sum_L \sum_{p=0,1} i^L \sqrt{2L+1} (i\lambda)^\pi \mathbf{A}_{L\lambda}^p, \quad (10)$$

where we introduce the standard notations $\mathbf{A}_{L\lambda}^{p=0,1}$ for the magnetic and electric multipole components, correspondingly.

By making use of two multipole expansions (9) and (10) together with the Wigner-Eckart theorem, we can rewrite the intermediate-state density matrix in the form

$$\begin{aligned} & \langle \alpha_f J_f M_f, \mathbf{p}m_s | \hat{\rho}_f | \alpha_f J_f M'_f, \mathbf{p}m'_s \rangle \\ &= \frac{2\pi}{2J_i + 1} \sum_{LL'pp'} \sum_{JJ'MM'} \sum_{\kappa\kappa'm_jm'_j} \sum_{\lambda\lambda'} c_{\lambda\lambda'} i^{l'-l+L-L'} \\ & \quad \times e^{i(\Delta_\kappa - \Delta_{\kappa'})} (i\lambda)^p (-i\lambda')^{p'} \frac{[L, L']^{1/2}}{[J, J']^{1/2}} \langle lm_l 1/2m_s | jm_j \rangle \\ & \quad \times \langle l'm'_l 1/2m'_s | j'm'_j \rangle Y_{lm_l}(\hat{\mathbf{p}}) Y_{l'm'_l}^*(\hat{\mathbf{p}}) \langle J_f M_f jm_j | JM \rangle \\ & \quad \times \langle J_f M'_f j'm'_j | J'M' \rangle \langle J_i M_i L\lambda | JM \rangle \langle J_i M_i L'\lambda' | J'M' \rangle \\ & \quad \times \left\langle (\alpha_f J_f, \epsilon l j) J \left\| \sum_n \boldsymbol{\alpha}_n \cdot \mathbf{A}_{L,n}^p \right\| \alpha_i J_i \right\rangle \\ & \quad \times \left\langle (\alpha_f J_f, \epsilon l' j') J' \left\| \sum_n \boldsymbol{\alpha}_n \cdot \mathbf{A}_{L',n}^{p'} \right\| \alpha_i J_i \right\rangle^*, \end{aligned} \quad (11)$$

where $[a, b, \dots] = (2a+1)(2b+1)\dots$ and $\langle (\alpha_f J_f, \epsilon l j) J | \sum_n \boldsymbol{\alpha}_n \cdot \mathbf{A}_{L,n}^p | \alpha_i J_i \rangle$ is the (multipole) reduced matrix element.

The intermediate-state density matrix (11) still contains the *complete* information about the overall system that consists of the emitted photoelectron and the (excited) ion. It can be used, therefore, to separate the density matrices of the individual subsystems and to obtain their reduced matrices. If we suppose, for example, that the photoelectrons remain unobserved in a particular experiment, the density matrix of the residual ion,

$$\begin{aligned} & \langle \alpha_f J_f M_f | \hat{\rho}_{\text{ion},f} | \alpha_f J_f M'_f \rangle \\ &= \sum_{m_s} \int d\Omega_p \langle \alpha_f J_f M_f, \mathbf{p}m_s | \hat{\rho}_f | \alpha_f J_f M'_f, \mathbf{p}m_s \rangle, \end{aligned} \quad (12)$$

is obtained by taking the trace over (the direction and the polarization states of) the electrons.

The reduced density matrix (12) describes the ion state $| \alpha_f J_f \rangle$ following the inner-shell photoionization and can be

employed to accompany the system through the subsequent characteristic photon emission. In order to investigate the angular and polarization properties of the characteristic light, however, it is often more convenient to represent the intermediate state of the ions in terms of the so-called statistical tensors:

$$\rho_{kq}(\alpha_f J_f) = \sum_{M_f M'_f} (-1)^{J_f - M'_f} \langle J_f M_f J_f - M'_f | kq \rangle \times \langle \alpha_f J_f M_f | \hat{\rho}_{\text{ion},f} | \alpha_f J_f M'_f \rangle. \quad (13)$$

Although both the reduced density matrix (12) and the statistical tensors (13) are mathematically equivalent, the latter form can be transformed similar to the spherical harmonics of rank k under a rotation of the coordinates [1,3,29]. In the next section, we will make use of these transformation properties in order to describe the magnetic sublevel population of the excited ions for two different choices of quantization axis.

Combining definition (13) with the reduced density matrix (12) and using some Racah algebra, the statistical tensors of the excited ionic states can be finally written as

$$\begin{aligned} \rho_{kq}(\alpha_f J_f) &= \frac{\pi}{2J_i + 1} \sum_{LL'pp'} \sum_{\kappa JJ'} \sum_{\lambda\lambda'} [\delta_{\lambda\lambda'} (1 + \lambda P_3) \\ &+ (1 - \delta_{\lambda\lambda'}) (P_1 - i\lambda P_2)] i^{L-L'+p-p'} \lambda^p \lambda'^{p'} \\ &\times [L, L', J, J']^{1/2} (-1)^{(J+J'+J_f+J_i+j+1)} \\ &\times \langle L\lambda L' - \lambda' | kq \rangle \left\{ \begin{matrix} J_f & j & J' \\ J & k & J_f \end{matrix} \right\} \left\{ \begin{matrix} J' & J_i & L' \\ L & k & J \end{matrix} \right\} \\ &\times \left\langle (\alpha_f J_f, \epsilon l j) J \left\| \sum_n \alpha_n \cdot \mathbf{A}_{L,n}^p \right\| \alpha_i J_i \right\rangle \\ &\times \left\langle (\alpha_f J_f, \epsilon l j) J' \left\| \sum_n \alpha_n \cdot \mathbf{A}_{L',n}^{p'} \right\| \alpha_i J_i \right\rangle^*, \end{aligned} \quad (14)$$

where, in addition, we have now expressed coefficients $c_{\lambda\lambda'}$ in terms of the polarization Stokes parameters [cf. Eq. (3)].

In the theory of atomic collisions, the statistical tensors (14) are often renormalized with respect to the zero-rank tensor [1,2]:

$$\mathcal{A}_{kq}(\alpha_f J_f) = \frac{\rho_{kq}(\alpha_f J_f)}{\rho_{00}(\alpha_f J_f)}. \quad (15)$$

These so-called reduced tensors (or alignment parameters) are then independent of the particular normalization of the ion density matrix. Moreover, their components with zero projection, $\mathcal{A}_{k0}(\alpha_f J_f)$, are directly related to the partial cross sections $\sigma_{M_f} \equiv \sigma_{\alpha_f J_f M_f}$ for the population of the individual ionic substates $|\alpha_f J_f M_f\rangle$:

$$\begin{aligned} \mathcal{A}_{k0}(\alpha_f J_f) &= \frac{\sqrt{2J_f + 1}}{\sigma(\alpha_f J_f)} \sum_{M_f} (-1)^{J_f - M_f} \\ &\times \langle J_f M_f J_f - M_f | k0 \rangle \sigma(\alpha_f J_f M_f), \end{aligned} \quad (16)$$

where $\sigma(\alpha_f J_f) = \sum_{M_f} \sigma(\alpha_f J_f M_f)$ denotes the total ionization cross section [29].

B. Inner-shell ionization by linearly polarized light

Equation (14) represents the general form of the statistical tensors of the ion in its intermediate state; it has been derived for an arbitrary polarization of the incident radiation and for the quantization axis chosen along the photon momentum \mathbf{k} . If we assume that incoming photons are linearly polarized along the x axis and with some degree of polarization $0 \leq P \leq 1$, the statistical tensors read

$$\begin{aligned} \rho_{kq}(\alpha_f J_f) &= \frac{\pi}{2J_i + 1} \sum_{LL'pp'} \sum_{\kappa JJ'} \sum_{\lambda\lambda'} i^{L-L'+p-p'} \lambda^p \lambda'^{p'} [L, L', J, J']^{1/2} \\ &\times [\delta_{\lambda\lambda'} + (1 - \delta_{\lambda\lambda'}) P] (-1)^{J+J'+J_f+J_i+j+1} \\ &\times \langle L\lambda L' - \lambda' | kq \rangle \left\{ \begin{matrix} J_f & j & J' \\ J & k & J_f \end{matrix} \right\} \left\{ \begin{matrix} J' & J_i & L' \\ L & k & J \end{matrix} \right\} \\ &\times \left\langle (\alpha_f J_f, \epsilon l j) J \left\| \sum_n \alpha_n \cdot \mathbf{A}_{L,n}^p \right\| \alpha_i J_i \right\rangle \\ &\times \left\langle (\alpha_f J_f, \epsilon l j) J' \left\| \sum_n \alpha_n \cdot \mathbf{A}_{L',n}^{p'} \right\| \alpha_i J_i \right\rangle^*. \end{aligned} \quad (17)$$

As seen from this relation and from the symmetry properties of the Wigner 6- j symbols, the statistical tensors $\rho_{kq}(\alpha_f J_f)$ are nonvanishing only if the rank k is even and if it satisfies the condition $k \leq 2J_f$. Moreover, for each $k \geq 2$, only the components (of statistical tensors) with $q = 0$ and $q = \pm 2$ may appear to be nonzero. These tensor components behave, however, in a different way with respect to the polarization P of incident radiation P . While the component with zero projection $q = 0$ is independent of the polarization, the two components with $q = \pm 2$ are proportional to P and, hence, vanish for the inner-shell ionization by an unpolarized photon beam.

As we mentioned already, Eqs. (14)–(17) have been derived for a particular “geometry” of the inner-shell ionization experiment in which the quantization (z) axis was adopted along the incoming photon momentum \mathbf{k} . By using such a geometry, one is able to explore the inner-shell ionization by an arbitrary polarized or even an unpolarized light. However, if the incoming radiation is *linearly* polarized, it is usually more convenient to choose the z axis along the photon polarization vector ϵ (see right panel of Fig. 1). There is no need to rederive again general expressions for statistical tensors $\tilde{\rho}_{kq}(\alpha_f J_f)$ in this new geometry. Instead, we just make use of the tensor transformation rules [2]. That is, under the rotation of the quantization axis from the \mathbf{k} to the ϵ direction, statistical tensors of the intermediate ionic state $|\alpha_f J_f\rangle$ transform as

$$\tilde{\rho}_{kq'}(\alpha_f J_f) = \sum_q D_{qq'}^k(0, \pi/2, 0) \rho_{kq}(\alpha_f J_f), \quad (18)$$

where $D_{qq'}^k(0, \theta, 0) = d_{qq'}^k(\theta)$ is the Wigner D function. By inserting Eq. (17) into this transformation relation and by making some angular momentum algebra, we find

$$\begin{aligned} \tilde{\rho}_{kq}(\alpha_f J_f) &= \frac{2\pi}{2J_i + 1} \sum_{LL'pp'} \sum_{\kappa JJ'} i^{L-L'+p-p'} [L, L', J, J']^{1/2} \\ &\times (-1)^{J+J'+J_f+J_i+j+1} \left\{ \begin{matrix} J_f & j & J' \\ J & k & J_f \end{matrix} \right\} \left\{ \begin{matrix} J' & J_i & L' \\ L & k & J \end{matrix} \right\} \end{aligned}$$

$$\begin{aligned}
& \times [d_{0q}^k(\pi/2)\langle L1L' - 1|k0\rangle + (-1)^{p'} \\
& \times P d_{2q}^k(\pi/2)\langle L1L'1|k2\rangle] \\
& \times \left\langle (\alpha_f J_f, \epsilon l j) J \left\| \sum_n \alpha_n \cdot \mathbf{A}_{L,n}^p \right\| \alpha_i J_i \right\rangle \\
& \times \left\langle (\alpha_f J_f, \epsilon l j) J' \left\| \sum_n \alpha_n \cdot \mathbf{A}_{L',n}^{p'} \right\| \alpha_i J_i \right\rangle^*, \quad (19)
\end{aligned}$$

and that the magnetic sublevel population of the excited ionic states is characterized by the statistical tensors of even rank k and its projection $q = 0, \pm 2$. However, if the incident radiation is completely polarized, i.e., $P = 1$, the decaying state gets aligned along the polarization vector of the incident photons. In this case, only the $q = 0$ components of the alignment tensor are nonzero.

C. Polarization of the decay photon

In the process of inner-shell photoionization, the residual ions appear to be in an excited state $|\alpha_f J_f\rangle$ which further decays to some lower state $|\alpha_0 J_0\rangle$ by the emission of a characteristic photon. To analyze the polarization properties of this decay radiation, it is useful to return to the density matrix representation and to utilize, once more, the relation $\hat{\rho}_0 = \hat{R} \hat{\rho}_{\text{ion},f} \hat{R}^\dagger$ [cf. Eq. (5)]. As before, the statistical operator $\hat{\rho}_0$ now describes both the ion in its final state $|\alpha_0 J_0\rangle$ as well as the characteristic (decay) photon with wave vector \mathbf{k}_0 and helicity λ , and in the representation of the individual momenta, the matrix of this operator can be obtained as

$$\begin{aligned}
& \langle \alpha_0 J_0 M_0, \mathbf{k}_0 \lambda | \hat{\rho}_\gamma | \alpha_0 J_0 M'_0, \mathbf{k}_0 \lambda' \rangle \\
& = \sum_{M_f M'_f} \langle \alpha_0 J_0 M_0, \mathbf{k}_0 \lambda | \hat{R} | \alpha_f J_f M_f \rangle \langle \alpha_f J_f M_f | \hat{\rho}_{\text{ion},f} \\
& \times | \alpha_f J_f M'_f \rangle \langle \alpha_f J_f M'_f | \hat{R}^\dagger | \alpha_0 J_0 M'_0, \mathbf{k}_0 \lambda' \rangle, \quad (20)
\end{aligned}$$

where $\langle \alpha_0 J_0 M_0, \mathbf{k}_0 \lambda | \hat{R} | \alpha_f J_f M_f \rangle$ is the transition matrix for the specific bound-bound radiative transition. In fact, this matrix element is similar to the bound-free transition amplitude as it appears in Eq. (7) but with the difference that both (many-electron) wave functions now represent bound ionic states on the left- and right-hand sides of the matrix element. From expression (20), the reduced density matrix of the characteristic photons can be obtained upon taking a trace over all unobserved quantum numbers of the ion in its final state and by performing partial-wave expansion of the electron-photon

interaction operator (6):

$$\begin{aligned}
& \langle \mathbf{k}_0 \lambda | \hat{\rho}_\gamma | \mathbf{k}_0 \lambda' \rangle \\
& = 2\pi \sum_{kq q'} D_{-qq'}^k(\hat{\mathbf{k}}_0) \rho_{kq}(\alpha_f J_f) \\
& \times \sum_{Lp L' p'} i^{L'-L+p'-p} \lambda^p \lambda'^{p'} [L, L']^{1/2} (-1)^{J_0+J_f+k+q+1} \\
& \times \langle L \lambda L' - \lambda' | k - q' \rangle \left\{ \begin{matrix} L & L' & k \\ J_f & J_f & J_0 \end{matrix} \right\} \\
& \times \left\langle \alpha_f J_f \left\| \sum_n \alpha_n \cdot \mathbf{A}_{L,n}^p \right\| \alpha_0 J_0 \right\rangle \\
& \times \left\langle \alpha_f J_f \left\| \sum_n \alpha_n \cdot \mathbf{A}_{L',n}^{p'} \right\| \alpha_0 J_0 \right\rangle^*. \quad (21)
\end{aligned}$$

This equation represents the most general form of the photon density matrix for the radiative transition between many-electron ionic states $|\alpha_f J_f\rangle$ and $|\alpha_0 J_0\rangle$. It depends both on the population of the excited ionic state as characterized by the set of tensorial components $\rho_{kq}(\alpha_f J_f)$ and on the electronic structure of a particular ion as reflected by the (reduced) matrix elements for the specified bound-bound multipole transition. In general, Eq. (21) includes the summation over all the different allowed multipoles (Lp) owing to the parity and angular momentum selection rules. For the decay to a $J_0 = 0$ state, of course, only one multipole component with multipolarity $L = J_f$ remains and leads to a significant simplification of the photon density matrix:

$$\begin{aligned}
& \langle \mathbf{k}_0 \lambda | \hat{\rho}_\gamma | \mathbf{k}_0 \lambda' \rangle \\
& = 2\pi (-1)^{1+J_f} \sum_{kq q'} D_{-qq'}^k(\hat{\mathbf{k}}_0) \rho_{kq}(\alpha_f J_f) (\lambda \lambda')^p \\
& \times \langle J_f - \lambda J_f \lambda' | k q' \rangle \left\langle \alpha_f J_f \left\| \sum_n \alpha_n \cdot \mathbf{A}_{L,n}^p \right\| \alpha_0 J_0 \right\rangle^2. \quad (22)
\end{aligned}$$

As discussed in Sec. III A, it is usually more convenient to express elements of the photon spin-density matrix in terms of polarization Stokes parameters. By combining the final-state density matrix (22) and the definition (3), we find the first Stokes parameter P_1 of the photons emitted in the $J_f \rightarrow J_0 = 0$ decay:

$$P_1(\hat{\mathbf{k}}_0) = \frac{(-1)^{1+J_f+P} [J_f]^{1/2} \frac{1}{2} \sum_{q=0, \pm 2} A_{kq}(\alpha_f J_f) (D_{-q2}^k(\hat{\mathbf{k}}_0) + D_{-q-2}^k(\hat{\mathbf{k}}_0)) \langle J_f 1 J_f 1 | k 2 \rangle}{1 + (-1)^{1+J_f} [J_f]^{1/2} \sum_{q=0, \pm 2} A_{kq}(\alpha_f J_f) D_{-q0}^k(\hat{\mathbf{k}}_0) \langle J_f 1 J_f - 1 | k 0 \rangle}, \quad (23)$$

where $A_{kq}(\alpha_f J_f)$ is given by Eq. (15).

As seen from Eq. (23), Stokes parameter $P_1(\hat{\mathbf{k}}_0)$ depends on the photon emission angles as well as on the alignment parameters A_{kq} , but it appears to be independent of the

bound-bound transition reduced matrix elements. Analysis of the polarization properties of characteristic $J_f \rightarrow J_0 = 0$ lines may provide, therefore, unambiguous information on the magnetic sublevel population of excited ions as produced

by means of inner-shell photoionization. To extract this information, one has to take care about the particular choice of the quantization (z) axis with respect to which both the set of reduced statistical tensors [cf. Eqs. (17) and (19)] and the

photon emission angles $\hat{\mathbf{k}}_0 = (\theta_0, \phi_0)$ need to be defined. For our two choices of the quantization axes as shown in Fig. 1, we find for the dipole transition $J_f = 1 \rightarrow J_0 = 0$ following the inner-shell ionization by linearly polarized light:

$$P_1 = \frac{(-1)^{1+J_f+p} [J_f]^{1/2} \frac{1}{2} \left[\sqrt{\frac{3}{2}} \mathcal{A}_{20}(\alpha_f J_f) - \mathcal{A}_{22}(\alpha_f J_f) \right] \langle J_f 1 J_f 1 | 22 \rangle}{1 + (-1)^{J_f} [J_f]^{1/2} \left[\frac{1}{2} \mathcal{A}_{20}(\alpha_f J_f) + \sqrt{\frac{3}{2}} \mathcal{A}_{22}(\alpha_f J_f) \right] \langle J_f 1 J_f - 1 | 20 \rangle}, \quad (24)$$

where the statistical tensors are still given by Eqs. (17) and (19). Moreover, in Eq. (24) we assume that the characteristic photons are observed in the direction *perpendicular* to the reaction (xz) plane as defined by the wave vector $\hat{\mathbf{k}}$ and polarization vector $\boldsymbol{\epsilon}$ of incident photons (see Fig. 1). In this case, the second Stokes parameter P_2 vanishes identically for this transition.

A slightly simpler expression for the Stokes parameter P_1 of the dipole radiation as measured perpendicular to the reaction plane can be obtained if one assumes the quantization axis along the polarization vector of incoming photons and ionizing radiation to be fully polarized:

$$P_1 = \frac{(-1)^{J_f+p} [J_f]^{1/2} \frac{1}{2} \sqrt{\frac{3}{2}} \tilde{\mathcal{A}}_{20}(\alpha_f J_f) \langle J_f 1 J_f 1 | 22 \rangle}{1 + (-1)^{J_f} [J_f]^{1/2} \frac{1}{2} \tilde{\mathcal{A}}_{20}(\alpha_f J_f) \langle J_f 1 J_f - 1 | 20 \rangle}. \quad (25)$$

Here, the alignment parameters are defined as $\tilde{\mathcal{A}}_{kq} = \tilde{\rho}_{kq} / \tilde{\rho}_{00}$ with $\tilde{\rho}_{kq}$ given by Eq. (19). Since the *observable* polarization properties of the characteristic light are independent of the particular choice of the quantization axis, Eqs. (24) and (25) must provide equivalent results for the Stokes parameter P_1 . This can be proved also rigorously by making use of the transformation relation (18) for the statistical tensors.

As seen from Eqs. (24) and (25), polarization properties of the dipole $J_f = 1 \rightarrow J_0 = 0$ radiation are defined by the second-rank tensors that contain the complete information on the magnetic sublevel population of the $|\alpha_f J_f = 1\rangle$ ionic state. Several additional fourth-rank parameters are required if we wish to describe the alignment of ions with $J_f = 2$. For the inner-shell ionization of highly charged ions, however, our theoretical calculations show that the parameters \mathcal{A}_{4q} are negligible in all considered cases. Therefore, one can still employ Eqs. (24) and (25) by taking $J_f = 2$ for the following analysis of the polarization properties of the quadrupole $J_f = 2 \rightarrow J_0 = 0$ radiation.

IV. COMPUTATIONS

From Eqs. (17)–(19) and (24)–(25), we see that all the alignment and Stokes parameters can be traced back to the computations of the (multipole) many-electron amplitudes $\langle (\alpha_f J_f, \ell j) J | \sum_n \boldsymbol{\alpha}_n \cdot \mathbf{A}_{L,n}^\pi | \alpha_i J_i \rangle$. These amplitudes describe the electron-photon interaction of an ionic bound state with the (one-electron) continuum of the next higher charge state. Following our previous work [15,30], these matrix elements have been evaluated by means of the multiconfiguration Dirac-Fock (MCDF) approach. Within such an approach, any

ionic bound state with angular momentum and parity (J^P) is approximated by a linear combination of the so-called configuration state functions (CSFs) of the same symmetry

$$\psi_\alpha(PJM) = \sum_{r=1}^{n_c} c_r(\alpha) |\gamma_r P J M\rangle, \quad (26)$$

where n_c is the number of CSFs and $\{c_r(\alpha)\}$ denotes the representation of the atomic state in this basis. In most standard computations, the CSFs are constructed as antisymmetrized products of a common set of orthonormal orbitals and are optimized on the basis of the Dirac-Coulomb Hamiltonian. Further relativistic contributions to the representation $\{c_r(\alpha)\}$ of the atomic states are then added later, owing to the given requirements, by diagonalizing the Dirac-Coulomb-Breit Hamiltonian matrix in first-order perturbation theory [31]. Especially for highly charged ions, the MCDF method has been found to be a versatile tool to account for the relativistic and many-body effects on the same footing, although the main insight can often be obtained already from the single configuration notation, i.e., the independent-particle model [32].

V. RESULTS AND DISCUSSION

In Sec. III C, we derived the basic formulas for the polarization Stokes parameter P_1 of the x-ray photons emitted following the inner-shell ionization of ions (or atoms) by linearly polarized light. As seen above, this parameter is uniquely defined by the set of reduced statistical tensors that characterizes the magnetic sublevel population of the excited ionic (or atomic) states. To investigate, therefore, the effect of the polarization of the incident light on the spin (polarization) states of the characteristic photons, we shall analyze first the polarization dependence of the alignment parameters of the intermediate ionic states $|\alpha_f J_f\rangle$. By following our previous work [15], we focus here on the $2p^5 3s$ states produced by means of an inner ionization of the $2p$ electron of sodiumlike Fe^{15+} , W^{63+} , and U^{81+} ions. For these ions, calculations were performed by adopting the quantization axis along (i) the momentum \mathbf{k} and (ii) the polarization vector $\boldsymbol{\epsilon}$ of the incoming photons; the statistical tensors for these two “geometries” are given by Eqs. (17) and (19), respectively.

As discussed in Sec. III B, three components of the reduced statistical tensor \mathcal{A}_{kq} with projections $q = 0, \pm 2$ are required in order to describe the population of the intermediate state

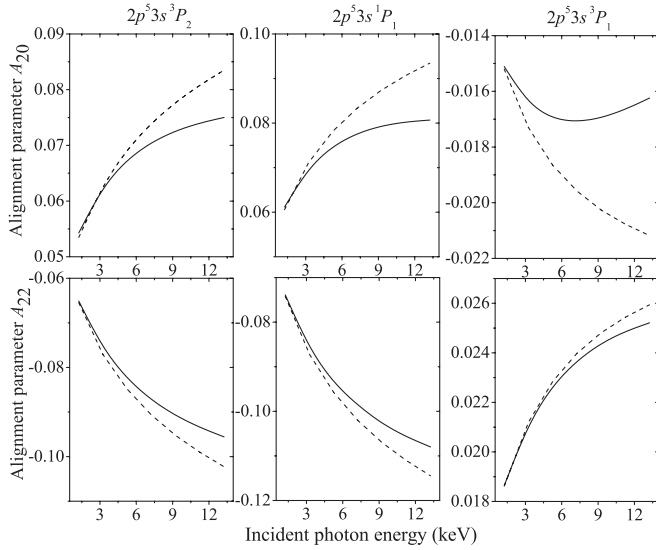


FIG. 2. Alignment parameters \mathcal{A}_{20} (top row) and \mathcal{A}_{22} (bottom row) of $2p^5 3s^3 P_2$ (left panels), $2p^5 3s^1 P_1$ (middle panels) and $2p^5 3s^3 P_1$ (right panels) states of neonlike Fe^{16+} ions following the inner-shell ionization by linearly polarized light. Solid and dashed lines represent results for the exact relativistic theory and the electric-dipole approximation, respectively. Calculations have been performed for the choice of quantization axis along the incoming photon momentum.

with the quantization axis taken along the incoming photon direction. For the inner-shell ionization by linearly polarized light, only two of these components are independent due to the relation $\mathcal{A}_{k+2} = \mathcal{A}_{k-2}$. In Fig. 2, we display the alignment parameters \mathcal{A}_{20} and \mathcal{A}_{22} for the $2p^5 3s^3 P_2$, $2p^5 3s^1 P_1$, and $2p^5 3s^3 P_1$ excited states of Fe^{16+} ions as a function of photon energies in the range $1.25 \leq \hbar\omega \leq 13.25$ keV. Since the component \mathcal{A}_{20} with zero projection is independent of the degree of polarization P of the incoming light and \mathcal{A}_{22} is expected to be proportional to P , the calculations have been performed for the beam of incident photons that is completely polarized in the x direction (cf. left panel of Fig. 1). As seen from the figure, this polarization leads to a nondiagonal density matrix of the intermediate ionic state and, hence, to a nonvanishing parameter \mathcal{A}_{22} . For the particular case of the $2p^5 3s^3 P_2$ and $2p^5 3s^1 P_1$ states, these parameters change from -0.0655 and -0.0742 for the near-threshold ionization to almost -0.1023 and -0.1145 for photon energy $\hbar\omega = 13.25$ keV, respectively. Therefore, the effect of the incoming photon polarization on the population of the photo-ion becomes more pronounced as the frequency of light is increased.

Besides the polarization transfer, we also investigated how in the inner-shell photoionization of ions, the nondipole relativistic effects influence the alignment of the excited ionic states. To explore these phenomena, we have performed calculations within both the exact relativistic theory that accounts for all allowed multipoles (Lp) in summation in Eq. (17) and the electric-dipole approximation as obtained by restricting the summation to $L = L' = 1$ and $p = p' = 1$, respectively. While, as expected, both approaches give rise to almost identical results near the ionization threshold, they start to differ as the photon energy is increased. The nondipole

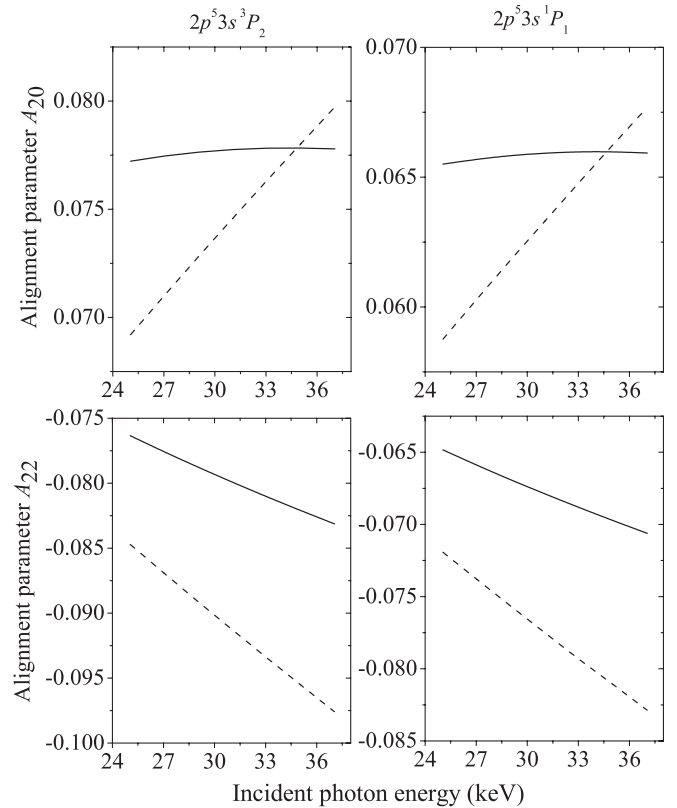


FIG. 3. Alignment parameters \mathcal{A}_{20} (top row) and \mathcal{A}_{22} (bottom row) of $2p^5 3s^3 P_2$ (left panels) and $2p^5 3s^1 P_1$ (right panels) states of neonlike U^{82+} ions following the inner-shell photoionization by linearly polarized radiation. Solid and dashed lines represent results for the exact relativistic theory and the electric-dipole approximation, respectively. Calculations have been performed for the choice of quantization axis along the incoming photon momentum.

contributions to the electron-photon interaction leads to a significant reduction of the alignment parameters for high photon energies. For the $2p^5 3s^3 P_2$ state and the energy $\hbar\omega = 13.25$ keV, for example, the components \mathcal{A}_{20} and \mathcal{A}_{22} are decreased by 10% and 7%, respectively, if the summation over the photon fields in Eq. (17) is not restricted to the dipole term.

Even stronger higher-multipole effects on the populations of the excited ionic states appear for the inner-shell ionization of (initially) sodiumlike U^{81+} ions. For these ions and for the photon energies in the range $25.05 \leq \hbar\omega \leq 37.05$ keV, we display in Fig. 3 the parameters \mathcal{A}_{20} and \mathcal{A}_{22} of the $2p^5 3s^3 P_2$ and $2p^5 3s^1 P_1$ excited states. No data are presented here for the population of $2p^5 3s^3 P_1$ state whose alignment was found to be negligible. Again, all calculations were performed within both the electric-dipole approximation and the exact relativistic theory which includes the complete summation over the higher multipoles in the electron-photon interaction and for completely polarized incoming light. As seen from the figure, higher multipole contributions strongly affect here the relative sublevel population already near the photoionization threshold. At the energy of $\hbar\omega = 25.05$ keV, for example, these contributions result in a 12% enhancement of the parameter \mathcal{A}_{20} and 10% reduction of (the absolute value of) \mathcal{A}_{22} .

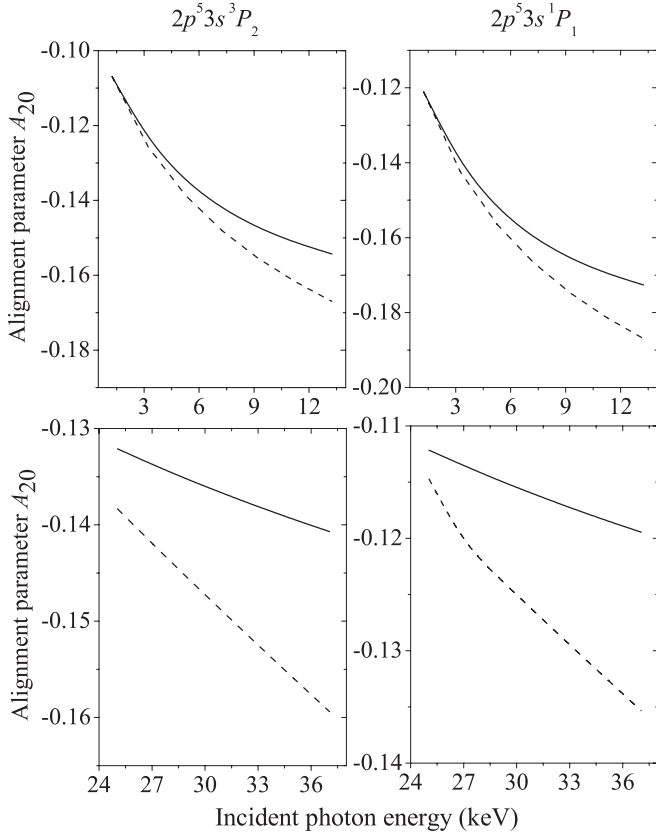


FIG. 4. Alignment parameter \tilde{A}_{20} of $2p^5 3s^3 P_2$ (left panels), $2p^5 3s^1 P_1$ (right panels) states of the (finally) neonlike Fe^{16+} (top row) and U^{82+} (bottom row) ions following the inner-shell ionization by linearly polarized radiation as a function of the incident photon energy. Solid and dashed lines represent results for the exact relativistic theory and the electric-dipole approximation, respectively. Calculations have been performed for the choice of quantization axis along the polarization vector ϵ of incoming photons.

Until now, we have discussed the alignment of the sodium-like Fe^{16+} and U^{82+} ions as defined with respect to the photon beam direction \mathbf{k} . As mentioned in Sec. III B, for the particular case of linearly polarized light, it is usually more convenient to use the photon polarization vector ϵ for the quantization axis of the system. For such a choice of the quantization axis, the magnetic sublevel population of the excited (photo-) ion is characterized by a single reduced statistical tensor \tilde{A}_{20} . The energy dependence of this parameter is displayed in Fig. 4 for the $2p^5 3s^3 P_2$ and $2p^5 3s^1 P_1$ excited states of Fe^{16+} and U^{82+} ions. Similar to Fig. 3, we do not present here the results for the $2p^5 3s^3 P_1$ level, whose alignment is almost zero. In contrast, the alignment parameters of the $^3 P_2$ and $^1 P_1$ states are nonvanishing and negative over all the energy range and point to a preferred population of the $M_J = 0$ substate with respect to the photon polarization direction [cf. Eq. (16)]. As can be expected from Fig. 1 and the transformation relation (18), such a magnetic sublevel population is opposite to that obtained for the quantization of the system along the incident photon momentum \mathbf{k} . For the latter, the photoionization process results in the dominant population of the $M_J = \pm 1$ levels and—as we have seen in Fig. 3—in a positive value of parameter A_{20} .

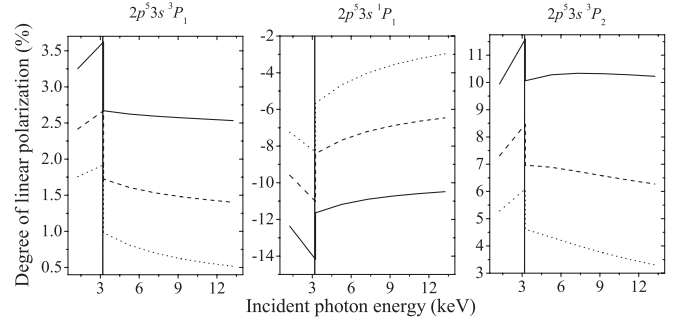


FIG. 5. Degree of linear polarization of the characteristic $2p^5 3s^3 P_1 \rightarrow 2p^6 \ ^1 S_0$ (left panel), $2p^5 3s^1 P_1 \rightarrow 2p^6 \ ^1 S_0$ (middle panel), and $2p^5 3s^3 P_2 \rightarrow 2p^6 \ ^1 S_0$ lines following the inner-shell ionization of the sodiumlike Fe^{15+} ions as a function of incident photon energy. Calculations have been performed within the exact relativistic theory and for three different degrees of incoming light polarization: $P_1^{\text{in}} = 0.1$ (dotted line), 0.5 (dashed line), and 1.0 (solid line). The dotted vertical line represents the onset of cascade feeding from higher-lying levels.

Of course, the particular choice of the quantization axis and, hence, the (set of) alignment parameters does not “affect” the observable properties—such as emission pattern and polarization—of the subsequent decay photons. Below we adopt the direction of the incident photon \mathbf{k} as the quantization axis in order to explore the linear polarization of the characteristic $2p^5 3s^3 P_1 \rightarrow 2p^6 \ ^1 S_0$, $2p^5 3s^1 P_1 \rightarrow 2p^6 \ ^1 S_0$, and $2p^5 3s^3 P_2 \rightarrow 2p^6 \ ^1 S_0$ lines following the inner-shell ionization of (initially) sodiumlike Fe^{15+} ions. The polarization Stokes parameter P_1 (24) for these lines, which are usually denoted in plasma spectroscopy as 3F, 3G, and 3H, is displayed in Fig. 5 as a function of the incident photon energy. Calculations have been performed within the exact relativistic theory for the statistical tensors (19), i.e., by taking into account all multipole components for the electron-photon interaction operator, and for the characteristic emission in the direction perpendicular to the plane spanned by the wave \mathbf{k} and polarization ϵ vectors. Moreover, to explore the polarization transfer in the two-step “ionization plus decay” process, Stokes parameter P_1 was evaluated for three different degrees of linear polarization of incoming light: $P_1^{\text{in}} = 0.1, 0.5,$ and 1.0 . As seen from the figure, linear polarization of all three characteristic lines enhances as the degree P_1^{in} increases from 0.1 to 1.0 (completely polarized light). In the particular case of the near-threshold ionization, for example, the polarization of incoming light leads to an increase of (the module of) the Stokes parameter P_1 from 1.75% to 3.25%, 7.23% to 12.36%, and 5.28% to 9.94% for the 3F, 3G, and 3H lines, respectively.

For a proper polarization analysis of the characteristic 3F, 3G, and 3H lines, one should incorporate also the cascade feeding from the higher-lying levels to the magnetic sublevels of the excited $2p^5 3s$ ion states. For the inner-shell photoionization of initially sodiumlike Fe^{15+} ions, cascade effects become important for the incoming photon energies $\hbar\omega > 3.25$ keV, i.e., beyond the $2s_{1/2}$ ionization threshold. In this energy range, the inner-shell photoionization process results in a significant population of the $2s 2p^6 3s \ ^1 S_{0,1}$ states, whose alignment, however, was found to be negligible. The

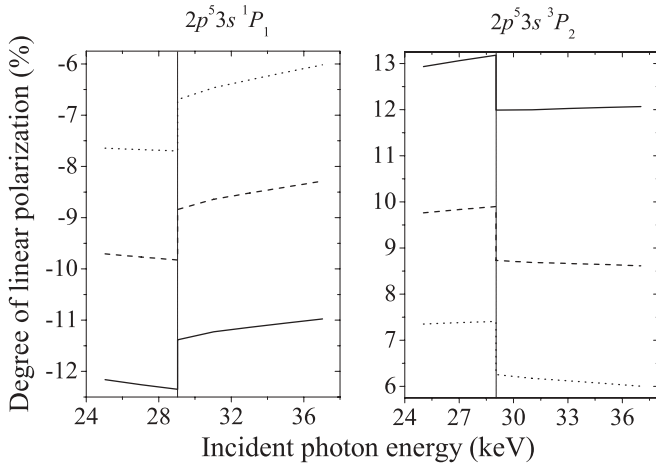


FIG. 6. Degree of linear polarization of the characteristic $2p^5 3s^1 P_1 \rightarrow 2p^6 1S_0$ (left panel) and $2p^5 3s^3 P_2 \rightarrow 2p^6 1S_0$ (right panel) x-ray lines following the inner-shell photoionization of sodiumlike U^{81+} ions as a function of incident photon energy. Calculations have been performed within the exact relativistic theory and for three different degrees of incoming light polarization: $P_1^{\text{in}} = 0.1$ (dotted line), 0.5 (dashed line), and 1.0 (solid line). The dotted vertical line represents the onset of cascade feeding from higher-lying levels.

radiative decay of these states to the lower-lying $2p^5 3s$ levels will result in a considerable reduction of the (absolute values of) alignment parameters $\mathcal{A}_{2q}(2p^5 3s)$ and, hence, in the depolarization of the characteristic x-ray lines [33]. In order to estimate *quantitatively* such an effect, a system of rate equations that describes the decay dynamics of the magnetic sublevels of the photo-ion has been integrated. By performing this integration, we found that the alignment of the $2p^5 3s^3 P_2$, $2p^5 3s^1 P_1$, and $2p^5 3s^3 P_1$ excited states of Fe^{16+} ions is reduced by 61%, 76%, and 83% if the cascade feeding is taken into account. As seen from Fig. 5, this causes 85%, 76%, and 63% depolarization of the 3F, 3G, and 3H lines, respectively.

Apart from the characteristic transitions in neonlike Fe^{16+} , we have also investigated the polarization properties of the 3G and 3H characteristic lines in U^{82+} ions. The Stokes parameter P_1 for these lines are displayed in Fig. 6 as a function of the incident photon energy. The parameter for the 3F line was found to not exceed 0.05% within the energy range $25.05 \leq \hbar\omega \leq 37.05$ keV and, hence, is not indicated here. Similar to the Fe^{15+} case, the degree of polarization of the other two lines, 3G and 3H, is strongly affected by the polarization state of incoming light. For the energy $\hbar\omega = 25.05$ keV, corresponding to the $2p_{3/2}$ ionization threshold, the Stokes parameters $P_1(3G)$ and $P_1(3H)$ increase almost by a factor of 2 and reach values of -12.16% and 12.93% if the $2p$ inner-shell vacancy is produced by a completely polarized photon beam. At higher incident photon energies, however, a strong depolarization of the characteristic radiation is observed and can be attributed again to the cascade feeding from the higher-lying levels.

In the discussion above, we have restricted ourselves to the $2p$ ionization and subsequent radiative stabilization of the (initially) sodiumlike Fe^{15+} and U^{81+} ions. Apart from these well-established examples, recent attention has been

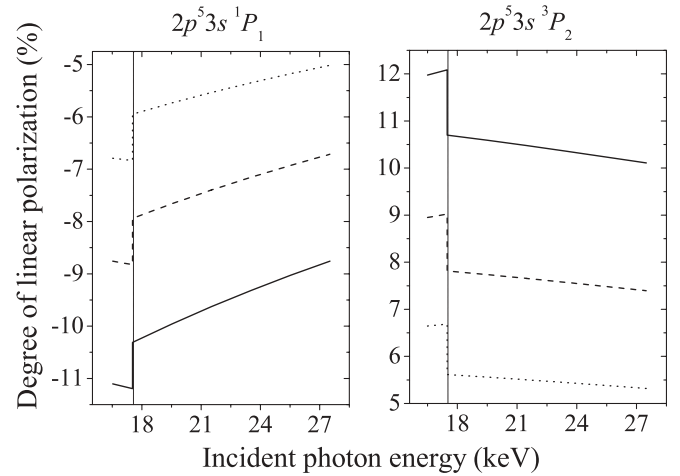


FIG. 7. Degree of linear polarization of the characteristic $2p^5 3s^1 P_1 \rightarrow 2p^6 1S_0$ (left panel) and $2p^5 3s^3 P_2 \rightarrow 2p^6 1S_0$ (right panel) x-ray lines following the inner-shell photoionization of sodiumlike W^{63+} ions as a function of incident photon energy. Calculations have been performed within the exact relativistic theory and for three different degrees of incoming light polarization: $P_1^{\text{in}} = 0.1$ (dotted line), 0.5 (dashed line), and 1.0 (solid line). The dotted vertical line represents the onset of cascade feeding from higher-lying levels.

paid also to the inner-shell ionization of tungsten sodiumlike ions. Tungsten—having the highest melting point of any metal—is likely to be used in some high-strength structural components in the experimental ITER fusion reactor which is under construction in France [34]. Detailed analysis of the characteristic radiation following excitation of highly charged tungsten ions can provide, therefore, valuable information about the fusion plasma conditions. In this contribution, we have explored the polarization properties of the 3G and 3H transitions in (finally) neonlike W^{64+} ions produced by means of $2p$ photoionization. Figure 7 displays, for example, the Stokes parameter P_1 for these lines as a function of the incident photon energy. Similar to the U^{82+} case, we do not show the P_1 parameter for the 3F line since it was found to be less than 1% within the energy range $16.50 \leq \hbar\omega \leq 27.50$ keV. In contrast, significant polarization of about 11–13% can be observed for the 3G and 3H lines if the incident photon beam is completely polarized.

Until now, we have employed expressions (14)–(23) for statistical tensors and Stokes parameter in order to investigate the linear polarization of the characteristic photons following the $2p$ vacancy production in sodiumlike ions. These general expressions can be utilized, of course, for an analysis of characteristic lines from other isoelectronic sequences. As an example, we consider here the $2p$ photoionization of initially magnesiumlike U^{80+} ions leading to the subsequent $2p^5 3s^2 2P_{3/2} \rightarrow 2p^6 3s^2 S_{1/2}$ decay. In order to study the polarization properties of this characteristic line, we use Eq. (21) and evaluate the Stokes parameter P_1 in the energy range $25 \leq \hbar\omega \leq 29$ keV. As seen from Fig. 8, the modulus of the Stokes parameter P_1 increases from 13.85% to 26.76% for the near-threshold ionization as the degree P_1^{in} increases from 0.1 to 1.0. Similar effect of polarization transfer has been discussed already for the sodiumlike ions. In contrast

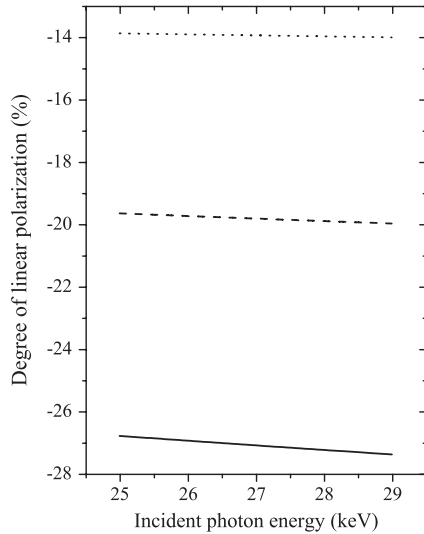


FIG. 8. Degree of linear polarization of the characteristic $2p^5 3s^2 2P_{3/2} \rightarrow 2p^6 3s^2 S_{1/2}$ x-ray line following the inner-shell photoionization of magnesiumlike U^{80+} ions as a function of incident photon energy. Calculations have been performed within the exact relativistic theory and for three different degrees of incoming light polarization: $P_1^{\text{in}} = 0.1$ (dotted line), 0.5 (dashed line), and 1.0 (solid line).

to the calculations above, however, no depolarization of the characteristic $2P_{3/2} \rightarrow 2S_{1/2}$ line due to cascade effects has been taken into account here, since the feeding from the higher-lying levels becomes important only for higher energies than those presented in Fig. 8.

VI. SUMMARY

The density matrix formalism, based on Dirac's relativistic theory, has been applied to describe the inner-shell photoionization of many-electron ions and their subsequent radiative decay. In our theoretical analysis, particular emphasis was placed on the question of how the polarization of the incident light affects the linear polarization of the characteristic radiation. In order to explore such a "polarization transfer," we first derived the general expressions for the statistical tensors that are used to characterize the magnetic sublevel population of the ion following the vacancy (photo) production. For the subsequent radiative decay of the excited ionic states, these tensors have been employed to obtain the polarization properties of the characteristic photons.

While the derived expressions can be applied to *any* many-electron ion, independent of its particular shell structure, detailed computations have been carried out for the $2p$ photoionization of the sodiumlike Fe^{15+} , W^{63+} , and U^{81+} ions and the subsequent $2p^5 3s^3 P_1 \rightarrow 2p^6 1S_0$ (3F), $2p^5 3s^1 P_1 \rightarrow 2p^6 1S_0$ (3G), and $2p^5 3s^3 P_2 \rightarrow 2p^6 1S_0$ (3H) decays. For the near-threshold ionization by unpolarized incident light, the degrees of linear polarization of these three lines were found to be 1.59%, -6.63% , and 4.78% for Fe^{16+} and 0.02%, -7.11% and 6.08% for U^{82+} ions, respectively. This—relatively low—polarization is enhanced by factor of 2 if the incoming photons are prepared in a fully polarized state.

Our relativistic calculations clearly indicate that a polarization transfer in the inner-shell photoionization can be observed best at the near-threshold energies. As the energy of incoming photons is increased, a strong depolarization of the characteristic x-ray radiation happens due to the cascade feeding from the higher-lying levels to the magnetic sublevels of the excited $2p^5 3s$ ion states. These cascade contributions were found to reduce the (degree of the) linear polarization of 3F, 3G, and 3H lines by about 85% for Fe^{16+} and 19% for W^{64+} and U^{82+} ions.

Apart from sodiumlike ions, calculations have been also performed to analyze the Stokes parameter P_1 of characteristic radiation following the $2p$ vacancy production in magnesiumlike U^{80+} ions. Again, significant enhancement of the linear polarization of the characteristic $2p^5 3s^2 2P_{3/2} \rightarrow 2p^6 3s^2 S_{1/2}$ line owing to the polarization of incoming photon beam has been observed in the near-threshold energy region.

In conclusion, our theoretical studies indicate a considerable "polarization transfer" effect in the process of inner-shell photoionization of many-electron ions; an effect that becomes most pronounced for the near-threshold energies. We therefore hope that the study of the polarization transfer will serve as an important tool in the diagnostics of laboratory and astrophysical plasmas. Moreover, it will help to understand the inner-shell ionization measurements which are likely to be carried out in the near future due to the advancement in the setup of intensive radiation sources and x-ray detectors.

ACKNOWLEDGMENTS

L.S. and A.S. acknowledge support from the Helmholtz Gemeinschaft and GSI (Nachwuchsgruppe VH-NG-421). M.K.I. gratefully acknowledges the cordial hospitality of Physikalisches Institut of Heidelberg University for a two-week stay. S.F. acknowledges support by DFG (FR 1251/13-2).

- [1] K. Blum, *Density Matrix Theory and Applications*, 2nd ed. (Plenum, New York, 1996).
- [2] V. V. Balashov, A. N. Grum-Grzhimailo, and N. M. Kabachnik, *Polarization and Correlation Phenomena in Atomic Collisions* (Kluwer Academic/Plenum, New York, 2000).
- [3] E. G. Berezhko and N. M. Kabachnik, *J. Phys. B* **10**, 2467 (1977).
- [4] M. K. Inal and J. Dubau, *J. Phys. B* **20**, 4221 (1987).
- [5] K. J. Reed and M. H. Chen, *Phys. Rev. A* **48**, 3644 (1993).

- [6] P. Beiersdorfer, G. Brown, S. Utter, P. Neill, K. J. Reed, A. J. Smith, and R. S. Thoe, *Phys. Rev. A* **60**, 4156 (1999).
- [7] D. L. Robbins, A. Ya. Faenov, T. A. Pikuz, H. Chen, P. Beiersdorfer, M. J. May, J. Dunn, K. J. Reed, and A. J. Smith, *Phys. Rev. A* **70**, 022715 (2004).
- [8] D. L. Robbins, P. Beiersdorfer, A. Ya. Faenov, T. A. Pikuz, D. B. Thorn, H. Chen, K. J. Reed, A. J. Smith, K. R. Boyce, G. V. Brown, R. L. Kelley, C. A. Kilbourne, and F. S. Porter, *Phys. Rev. A* **74**, 022713 (2006).

- [9] Z. Bedrane, M. K. Inal, and S. Fritzsche, *J. Phys. B* **42**, 055701 (2009).
- [10] J. Jiang, C. Z. Dong, L. Y. Xie, and J. G. Wang, *Phys. Rev. A* **78**, 022709 (2008).
- [11] T. Kai, S. Nakazaki, T. Kawamura, H. Nishimura, and K. Mima, *Phys. Rev. A* **75**, 012703 (2007).
- [12] F. Wang, S. Fujioka, H. Nishimura, D. Kato, Y. Li, G. Zhao, J. Zhang, and H. Takabe, *Phys. Plasmas* **15**, 073108 (2008).
- [13] B. A. Remington, R. P. Drake, and D. D. Ryutov, *Rev. Mod. Phys.* **78**, 755 (2006).
- [14] F. Paerels, J. Cottam, M. Sako, D. A. Liedahl, A. C. Brinkman, R. L. J. van Der Meer, J. S. Kaastra, and P. Predehl, *Astrophys. J. Lett.* **533**, L135 (2000).
- [15] M. K. Inal, A. Surzhykov, and S. Fritzsche, *Phys. Rev. A* **72**, 042720 (2005).
- [16] F. Wang, S. Fujioka, H. Nishimura, D. Kato, Y. Li, G. Zhao, J. Zhang, and H. Takabe, *Phys. Plasmas* **15**, 073108 (2008).
- [17] J. J. MacFarlane, J. E. Bailey, G. A. Chandler, C. Deeney, M. R. Douglas, D. Jobe, P. Lake, T. J. Nash, D. S. Nielsen, R. B. Spielman, P. Wang, and P. Woodruff, *Phys. Rev. E* **66**, 046416 (2002).
- [18] J. E. Bailey *et al.*, *Phys. Plasmas* **9**, 2186 (2002).
- [19] J. E. Bailey *et al.*, *J. Quant. Spectrosc. Radiat. Transfer* **71**, 157 (2001).
- [20] A. S. Shlyaptseva, S. B. Hansen, V. L. Kantsyrev, B. S. Bauer, D. A. Fedin, N. Ouart, S. A. Kazantsev, A. G. Petrashen, and U. I. Safronova, *Rev. Sci. Instrum.* **72**, 1241 (2001).
- [21] S. V. Lebedev *et al.*, *Plasma Phys. Control. Fusion* **47**, A91 (2005).
- [22] D. Lai and W. C. G. Ho, *Phys. Rev. Lett.* **91**, 071101 (2003).
- [23] J. D. Schnittman and J. H. Krolik, *Astrophys. J.* **701**, 1175 (2009).
- [24] G. J. Ferland, *Annu. Rev. Astron. Astrophys.* **41**, 517 (2003).
- [25] A. Derevianko, W. R. Johnson, and K. T. Cheng, *At. Data Nucl. Data Tables* **73**, 153 (1999).
- [26] M. K. Inal, H. L. Zhang, and D. H. Sampson, *Phys. Rev. A* **46**, 2449 (1992).
- [27] J. Eichler and W. Meyerhof, *Relativistic Atomic Collisions* (Academic, San Diego, 1995).
- [28] M. E. Rose, *Elementary Theory of Angular Momentum* (Wiley, New York, 1953).
- [29] S. Fritzsche, A. Surzhykov, and Th. Stöhlker, *Phys. Rev. A* **72**, 012704 (2005).
- [30] S. Fritzsche, *J. Electron Spectrosc. Relat. Phenom.* **114-116**, 1155 (2001).
- [31] S. Fritzsche, C. Froese Fischer, and G. Gaigalas, *Comput. Phys. Commun.* **148**, 103 (2002).
- [32] A. Surzhykov, P. Koval, and S. Fritzsche, *Comput. Phys. Commun.* **165**, 139 (2005).
- [33] N. M. Kabachnik, S. Fritzsche, A. N. Grum-Grzhimailo, M. Meyer, and K. Ueda, *Phys. Rep.* **451**, 155 (2007).
- [34] <http://www.physorg.com/news171650049.html>